Smart Energy 21 (2026) 100227

Contents lists available at ScienceDirect

Smart Energy

journal homepage: www.journals.elsevier.com/smart-energy

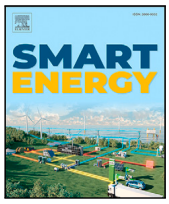

Analysis of bidirectional EV charging infrastructures within industrial DC grids☆

Henning Rahlf [a,*], Lukas Knorr [a], Simon Althoff [b], Henning Meschede [a]

[a] Department of Energy System Technologies, Paderborn University, Warburger Str. 100, 33098, Paderborn, North Rhine-Westphalia, Germany
[b] Technology Development, Weidmüller GmbH & Co. KG, Klingenbergstraße 26, 32758 Detmold, North Rhine-Westphalia, Germany

ARTICLE INFO

Keywords:
DC-grid
Droop control
Grid-serving behaviour
Grid stability
Bidirectional charging
Sequential decision
MILP optimisation

ABSTRACT

Industrial electrification is increasing to reduce fossil fuel dependence, alongside a growing share of volatile renewables. A secure and reliable energy supply is crucial for industry, leading to a shift from centralised to decentralised grid structures. DC microgrids becoming increasingly popular in industry, since they enable energy recuperation from braking, reduce components and cables, and integrate storage and local generation to manage supply interruptions or peak loads. EVs add further synergies by serving as mobile storage units, helping to store and redistribute locally generated renewable energy. This paper analyses how EV integration in droop-controlled DC grids can contribute to a more stable, low-emission and peak-reduced load profile to the supply grid through load shifting and bridge interruptions. A droop-controlled DC grid model has been developed, incorporating an EV charging park based on probability functions. Scalable scenarios allow for diverse condition analysis using an energy management system that utilises fuzzy logic and sequential MILP optimisation. It has been shown that a 7% improvement of coefficient represented grid-serving behaviour is possible by load shifting. It has also been demonstrated that an optimised EMS can reduce the demand-based CO_2 emissions by 41 kg for a representative day compared to a fuzzy logic EMS. At the same time peak load is decreased yielding a more constant residual load. These results highlight the potential of a controlled bidirectional charging infrastructure in DC grids and underscore the need to explicitly consider charging processes to ensure a residual load as constant as possible.

1. Introduction

A secure and reliable energy supply is crucial for industry, especially when continuous processes are running or safety-related equipment is operated. In order to secure this, direct current (DC) microgrids are becoming increasingly the focus of research [1] as they help to secure the energy supply and simultaneously reduce carbon dioxide (CO_2) emissions [2]. This is achieved by recovering braking energy and simplifying the integration of energy storage systems, among other things [3].

These grids connect various electrical producers and consumers within a company and are usually connected to the public distribution grid. The bidirectional coupling takes place via an active infeed converter (AIC). As many devices, storage systems and generators use direct current, a direct DC connection offers advantages. Energy can be exchanged between grid participants and locally generated renewable energy can be buffered in storage systems. In addition, there is no need for alternating direction and grid synchronisation.

In DC grids, the power balance is reflected by the grid voltage [4]. Maintaining this grid stability is a central challenge and the highest priority. One key strategy to ensure this is through droop control, which helps to balance the power flow and is widely used in DC microgrids [5]. While ensuring grid stability has the highest priority, energy management systems (EMS) can coordinate a grid-serving behaviour of the DC microgrid. This concept describes how a system contributes positively to the grid's operation, for example, by reducing bottlenecks or lowering the need for grid expansion. In general, grid-serving systems attempt to realise a balancing of the grid load or an adjustment between generation and demand [6]. To this end, the energy demand is adjusted to the renewable feed-in to minimise the fluctuation of the residual load [7].

Electric vehicles (EV) offer additional synergies as they have their own battery storage systems. They can be used as mobile, temporary energy storage units to store locally generated renewable energy and

☆ This article is part of a Special issue entitled: 'SESAAU2024' published in Smart Energy.

* Corresponding author.
E-mail addresses: henning.rahlf@uni-paderborn.de (H. Rahlf), lukas.knorr@uni-paderborn.de (L. Knorr), simon.althoff@weidmueller.com (S. Althoff), henning.meschede@uni-paderborn.de (H. Meschede).

https://doi.org/10.1016/j.segy.2026.100227
Received 28 February 2025; Received in revised form 13 January 2026; Accepted 26 January 2026
Available online 30 January 2026
2666-9552/© 2026 The Authors. Published by Elsevier Ltd. This is an open access article under the CC BY license (http://creativecommons.org/licenses/by/4.0/).

Glossary

Variables and Constants

c_{Energy}	Energy costs
E	Electrical energy (kW h)
E_{ESS}	Storage capacity (kW h)
E^{var}	Energy optimisation variable (kW h)
f_{α}	Probability density function of α
GSC^{T}_{ref}	Grid Support Coefficient
I, i	Electrical current (A)
k_{ref}	Grid-specific reference value
M	Big-M-Variable
m	Mass (kg)
m_{CO_2}	specific CO_2 emissions ($gCO_2eq\,kW^{-1}\,h^{-1}$)
P	Electrical power (W)
P^{opt}	Optimal power (kW)
P^{var}	Power optimisation variable (kW)
T	Time interval (s)
t	Time (s)
U, u	Electrical voltage (V)
W	Electrical work (J)
δ^{var}_{j}	Binary optimisation variable
η	Efficiency (%)
μ	Expected value

Acronyms

AC	Alternating Current
AIC	Active Infeed Converter
CO_2	Carbon dioxide
DC	Direct Current
EMS	Energy Management System
ESS	Energy Storage System
EV	Electric Vehicle
EVSE	Electrical Vehicle Supply Equipment
GSC	Grid Support Coefficient
LSTM	Long short-term Memory
MILP	Mixed Integer Linear Programming
PV	Photovoltaic
SoC	State of Charge
V2G	Vehicle to Grid
V2X	Vehicle to X

make it available later. The increasing share of EVs considering future mobility concepts can increase the efficiency of renewable energies in regional energy systems [8].

The greater the number of EVs, the greater the load on the supply grids, which increases the need to expand the grid [9]. One study emphasises that the maximum charging capacity and the strategic positioning of charging stations are decisive criteria for grid planning [10], while another study shows that uncontrolled charging of electric cars can lead to grid bottlenecks and local overloads, thus increasing the need for grid expansion and intelligent load management [11]. This highlights the need for intelligent load management and a grid-serving approach.

Vertgewall et al. [12] showed that controlled charging could drastically reduce grid reinforcement costs. *Gschwendtner et al.* [13] found workplace Vehicle-to-X (V2X) dominant due to centralised benefits, suggesting that there is considerable potential for load shifting and demand side management.

EMS are essential to ensure the efficient or optimised use of different grid participants in microgrids. To classify this *Shafiullah et al.* [14] provide an overview of current developments in management strategies in microgrids. They emphasise the need for an EMS to ensure grid stability. In their work on optimal energy planning in smart grids, *Khan et al.* [15] categorise and classify energy management strategies and make a distinction between rule-based and optimisation-based. They summarise that robust optimisation is crucial for the integration of renewable energies into current EV charging infrastructures and microgrids.

Optimisation is also used by *Dicorato et al.* [16] considering the day-ahead energy price to charge EVs in a price-controlled manner. By applying different scenarios, it was shown that the total costs of a day can be reduced by load shifting. In further work, the authors were able to show that purely monetary objective functions place a greater burden on the supply network, as charging processes are concentrated in times of low prices [17]. Against this background, the here presented paper develops a non-price-driven method. However, grid-serving utility is not taken into account, nor is industrial load considered. Another strategy was presented by *Bruinsma et al.* [18] in their work, with the main objective to optimise the charging of EVs while simultaneously generating photovoltaic (PV) energy. They used charging strategies to reduce the maximum power under given load condition from an external grid but also did not characterise grid-serving aspects.

In addition to work based on optimisations, fuzzy logic is often used for control purposes. *Shakeel* and *Malik* [19] used fuzzy logic to determine the available energy of individual EVs for vehicle-to-grid (V2G) services. In the context of DC grids, fuzzy logic is also used by *García-Triviño et al.* [20] to regulate the DC voltage and energy storage state of charge (SoC) while a separate study presents a decentralised fuzzy logic control method to ensure proper voltage and SoC thresholds under varying PV power and EV charging conditions [21].

The integration of renewable energies into energy systems poses new challenges in terms of grid reliability and security of supply. In this context, the alignment between local generation and load in the electrical systems is becoming increasingly important. Particularly in decentralised micro- and DC grids, which are characterised by fluctuating feeders and dynamic loads, the development of suitable control and energy management strategies is crucial to ensure reliable and stable operation that also serves the grid.

One key area of research focuses on the role of EVs as flexible loads. Under the concept of V2G or, more generally, V2X, researchers are investigating how EV batteries can be used not only as consumers but also as producers through bidirectional charging [22]. Several studies have already shown that V2X technologies can make a positive contribution to the stability and resilience of distribution grids and microgrids [23]. Another frequently used approach is a virtual synchronous generator, which allows frequency services to be provided via V2G [24]. Extending this line of research, *Li et al.* [25] analysed the impact of V2G control strategies on frequency regulation in microgrids. They concluded that EVs using a virtual synchronous generator based approach can provide effective frequency support while simultaneously meeting charging demands.

While existing work provides important insights into the potential of EVs in the context of energy and load management, research gaps remain. A systematic analysis of industrial DC microgrids with integrated EV charging systems is less common. Furthermore, there is a lack of consolidated consideration of various partial approaches. While droop control characteristics and EMS are already subject of research and large-scale EV fleets have shown their capability for frequency regulation [26], there is no analysis of the added value for grid-serving behaviour by using an EMS in industrial DC grids in combination with bidirectional charging of EVs.

Against this background, the aim and the novelty of this paper is to investigate the added value by an EMS to an industrial DC microgrid

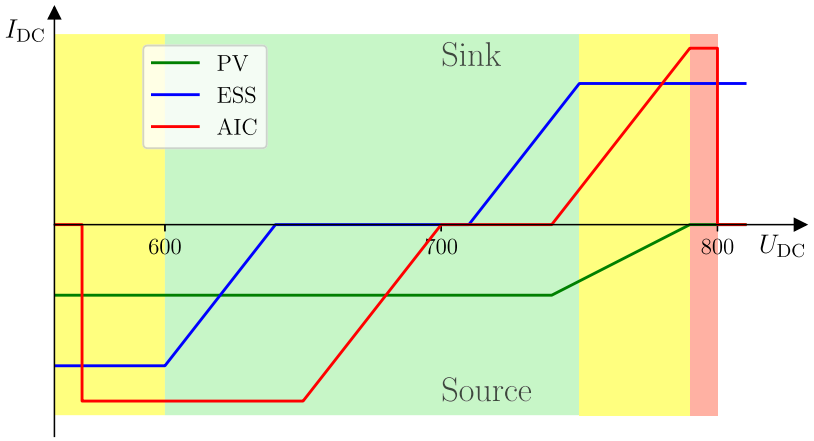

Fig. 1. Example of droop control characteristics in a DC grid according to [27]. Above the nominal voltage band (green), devices are allowed to reduce their power. The values of the currents are for illustrative purposes only.

with the integration of EV charging systems. The focus is on two aspects: firstly, the analysis of suitable EMS that integrate EVs into the DC grid as flexible, bidirectionally usable storage devices; secondly, the evaluation of demand side management capabilities under different load, design and failure scenarios. As a further contribution, CO_2 emissions are identified and employed as a predictable indicator for aligning local generation and demand to flatten the residual load, thereby extending the methodological novelty of this work. An additional added value lies in the simultaneous reduction of emissions. For this reason, the paper concludes with an examination of load adjustment potential and environmental impacts.

The results should provide a base for developing robust control methods that enable the reliable, efficient, and grid-serving integration of EVs into industrial DC microgrids.

This paper is structured as follows: Section 2.1 presents how energy management works in DC grids and how a droop-controlled DC grid is structured. Two models for generating setpoints based on fuzzy logic (Section 2.2.2) and based on linear mixed-integer optimisation (Section 2.2.3) are then presented. Based on a case study (Section 2.3), simulation results of the implemented EMS are presented and analysed in Section 3. Finally, the findings are discussed in Section 4 and summarised.

2. Methods

This chapter presents the methods for control and the use of an EMS in droop-controlled industrial DC grids. First, the fundamental structure and control strategy of DC grids are described, distinguishing between active and passive participants. Second, it is shown how a load profile can be evaluated in terms of a constant residual load. Subsequently, the derivation of two EMSs for setpoint generation in bidirectional charging is explained: a rule based fuzzy logic control and a sequentially optimised mixed integer linear programming (MILP) model. Finally, a specific DC grid is introduced as a case study to illustrate the practical application of the developed methods. A DC grid model in MATLAB® and Simulink® is used for the simulations and optimisation.

2.1. Droop control in industrial DC grids

For stable DC grid operation, the grid voltage must remain within a defined range, which is controlled by droop control characteristics. The current to be fed in or drawn is adjusted depending on the voltage (see Fig. 1). With negative currents, the devices act as a source, with positive currents as a sink. The AIC requires a minimum voltage above the rectified alternating current (AC) voltage, which in a 400 V AC grid corresponds to approximately 565 V. The upper limit is 800 V according to the definition of DC voltage bands in [28], whereby all participants must absorb energy or stop feeding it in. The energy storage system (ESS) remains inactive in the nominal voltage range and only feeds in at low voltage. When the voltage rises, it absorbs energy before the AIC feeds it back into the AC grid. The PV system only feeds in and only reduces its feed-in when the voltage is too high. Devices with a droop control characteristic are considered active, loads are considered passive devices. However, ESS and PV systems cannot always follow the droop control characteristic as they depend on external or internal conditions. Therefore, the ESS has a secondary SoC controller that superimposes the setpoint current on the primary control characteristic [27]. For further explanations, please refer to *Ehlich et al.* [29] and *Ott et al.* [30].

2.2. Setpoint generation for bidirectional charging in DC grids

This section presents two approaches to energy management in the DC grid. The focus is on grid-friendly operation of the DC grid with the integration of a bidirectional charging infrastructure for EVs. A fuzzy logic based and an optimisation based EMS are presented. Both approaches are based on shifting the droop control characteristics of the individual participants in the DC grid. By shifting, the operating point of a device can be changed while the control characteristic of the power flow controller remains active.

2.2.1. Evaluation of the grid-serving possibility of electrical systems

There are various ways to effect and evaluate grid-serving behaviour. A classic example is the provision of frequency containment reserve, which performs an essential function in large AC transmission grids for frequency stabilisation. In principle, this system service can also be technically supported by controllable units such as the AIC in DC grids. However, this is not suitable in practical industrial DC grids, as the energy density and power range of the systems are insufficient to make a significant contribution. In addition, DC grids mostly occur as consumers even with renewable energy supplies. An alternative is to adapt the power consumption to the availability of renewable energy, which reduces the residual load and simplifies grid operation [31]. In DC grids, demand side management is practically the only suitable mechanism to provide grid-supportive behaviour from within the microgrid. EVs as a major controllable load, offer significant potential for load shifting by adapting the charging demand to external conditions such as renewable generation or grid constraints. This effect can be further enhanced through bidirectional charging, which allows EV batteries not only to adjust their consumption but also to supply energy back to the grid when needed.

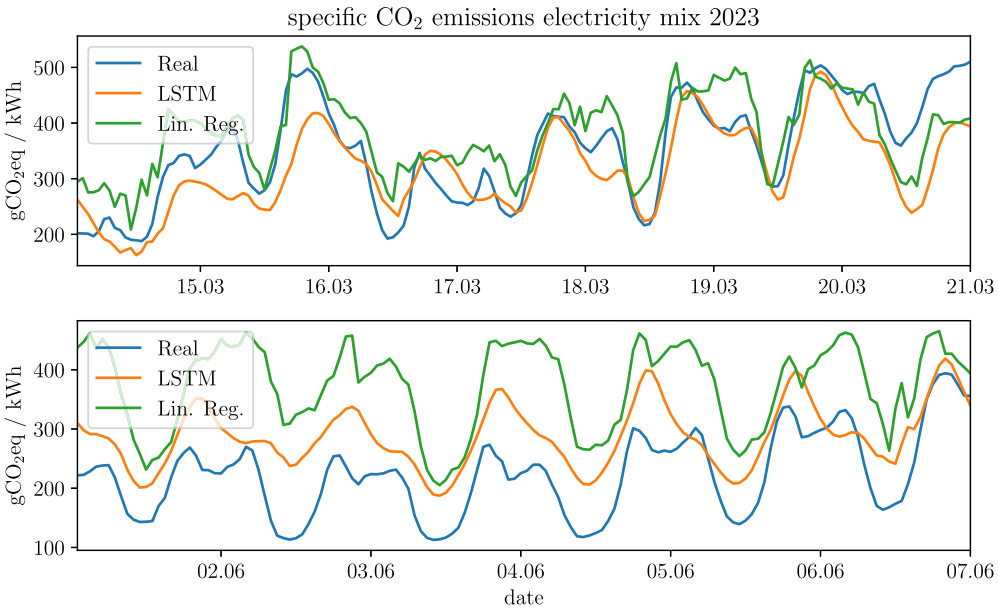

Fig. 2. Prediction of specific CO_2 emissions in the electricity mix for two exemplary weeks the year 2023.

Grid-serving behaviour can be achieved by smoothing the residual load through energy procurement via the AIC [32]. A more even residual load reduces the control effort required by power plant operators to ensure stable grid operation. Typical indicators for an optimal energy procurement are the electricity exchange price or the current CO_2 emissions in the electricity mix [33]. A self-conducted investigation of the specific CO_2 emissions on generation data from 2023 from the Association of European Transmission System Operators has shown that these correlate with the residual load ($r = 0.88$) and can therefore be used as a reference signal. Furthermore, it was demonstrated that CO_2 emissions can be predicted based on weather forecasts. To this purpose, two prediction models (a linear regression model and a long short-term memory (LSTM) model) were implemented and compared with each other. The prediction result for two sample weeks in 2023 is shown in Fig. 2. The upper diagram shows a week in March and the lower diagram a week in June. Although the prediction is not perfect, it reliably shows trends such as higher CO_2 emissions in the morning and evening and lower emissions at midday. In addition, the LSTM model predicts the emission level more accurately than the linear regression.

In order to assess whether a consumer is acting in a grid-serving manner in relation to the AC grid, a coefficient is used which was presented [31] and developed [34] by researchers at *Fraunhofer ISE*. This is the *Grid Support Coefficient* (GSC), with which a load profile can be evaluated dimensionless. To calculate the coefficient

$$GSC_{\text{ref}}^{T} = \frac{\int P_{\text{el}}(t) \cdot k_{\text{ref}}(t)\,\mathrm{dt}}{W_{\text{el}} \cdot \overline{k}_{\text{ref}}} \tag{1}$$

the product of the electrical power P_{el} and the grid-specific reference variable k_{ref} is integrated over the time t and divided by the product of the total energy consumption W_{el} and the averaged reference variable $\overline{k}_{\text{ref}}$. The result is a number that can be greater or less than one, whereby a constant load profile $P_{\text{el}}(t)$ is given the value $GSC_{\text{ref}}^{T} = 1$ by definition. A value greater than one means that a consumer predominantly draws energy at unfavourable times. The opposite applies for values less than one. The reference variable k_{ref} is used to determine whether the energy consumption is favourable or unfavourable in relation to a constant load. The coefficient can be determined for any time period and any reference variable. If a reference variable is selected that has high values precisely when energy consumption is unfavourable, high energy consumption during these phases will cause the numerator to be greater than the denominator. As a result, the GSC will assume a value greater than one. In this work, the specific CO_2 emissions are used as a reference value, as these can verifiably be used to achieve grid-serving behaviour by smoothing the residual load. Another positive side effect occurs at the same time through energy procurement during periods of low specific CO_2 emissions, as overall emissions are reduced.

2.2.2. Setpoint generation based on fuzzy logic

This EMS employs a fuzzy logic controller to determine setpoints for the AIC offset $i_{\text{AIC,offset}}$ and electric vehicle supply equipment (EVSE) scaling factor $p_{\text{EVSE,scale}}$. Key input variables are the DC grid voltage U_{DC} and the SoC of the ESS. The load current is the primary factor distinguishing between light and heavy load conditions; however, U_{DC} serves as a proxy for this information, decreasing with increasing load.

The fuzzy logic controller prioritises ESS charging under light load conditions, before curtailing feed-in power via the AIC. When the grid voltage is within an acceptable range and the ESS is not fully charged, excess renewable energy is directed towards charging EVs. Conversely, under heavy load, the ESS is discharged before the AIC increases feed-in power, providing immediate DC grid support.

The output variables, $i_{\text{AIC,offset}}$ and $p_{\text{EVSE,scale}}$, modulate the AIC droop control characteristic and EVSE output power, respectively. The membership functions of the input variables in Fig. A.17 and the associated fuzzy logic rules in Table A.1 are provided in Appendix A, so that the inputs to the outputs are as shown in Fig. 3. The left figure illustrates that the AIC control characteristic shifts primarily negatively at low to medium DC grid voltages, particularly when the ESS SoC is low to medium. A high SoC limits energy transfer via the AIC in these conditions. The figure on the right demonstrates that the EVSE scaling factor is positive or zero at medium to high grid voltages, facilitating EV charging. When the voltage is low, the factor becomes negative, enabling EVs to provide voltage support by discharging. Charging is prioritised when the ESS SoC is sufficient, while discharging from EVs is confined to operation near the minimum allowable DC voltage.

2.2.3. Setpoint generation based on sequential optimisation

In an EMS based on sequential optimisation, an optimisation problem is solved over a rolling horizon with a step size T_{step}, an execution interval T_{exec} and a horizon T_{hor}. This is used because predictions can deviate or change or unforeseen states can occur.

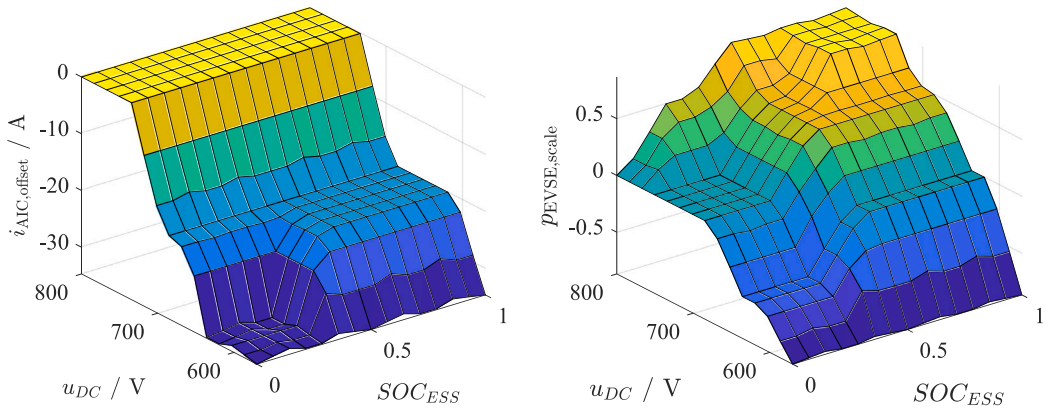

Fig. 3. Input–output behaviour of the fuzzy control for the two inputs U_{DC} and SoC_{ESS} as well as the outputs $i_{AIC,offset}$ and $p_{EVSE,scale}$.

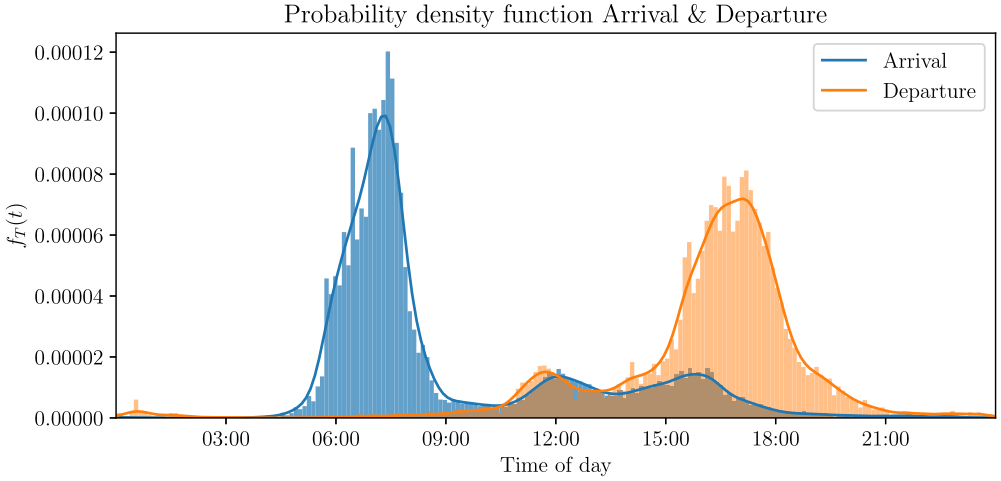

Fig. 4. Histogram and probability density function of arrival and departure of an EV at a charging station. Representation of data according to [35].

The sequential optimisation is also necessary as it is unclear which EVs are to be charged via the charging points in the DC grid. Depending on the SoC, battery capacity and availability, different power levels must be provided. Discharging is only possible under certain, time-varying conditions.

Vehicles arrive in the morning with a certain probability and usually leave in the late afternoon. In addition, some vehicles arrive or depart at midday. The probability density functions for arrival and departure, generated from a dataset based on [35], are shown in Fig. 4. However, as soon as a special charging park is realised, the times change. For this reason, it is necessary to consider the structure of the realisation for the prediction of the charging processes. There is a logical relationship between the number of EVSEs, the number of users and the time at which a charging station is typically occupied. In Fig. 5 the probability density functions of arrival at an EVSE are shown for different realisations. Two relationships are recognisable: the more EVSE are available, the later the arrival mode value, and the more users travelling to an EVSE, the earlier the mode value. The arrival mode value of a realisation is always less than or equal to the mode value of all possible arrivals, which is explained by the *first come, first served* principle. The stay time of an EV also shows a pattern: vehicles that arrive early stay longer, while vehicles that arrive between 15:00 and 18:00 stay shorter on average. Users who plug their vehicle in the evening often stay longer than users who plug in the afternoon. This is shown in Fig. 6 based on the piecewise linear interpolation of a data set of $N = 1$ million realisations, the mean stay time of an EV can be estimated based on the arrival time.

In sequential optimisation, two approaches are used to predict the capacity of the connected EVs. As long as a charging station is free, it is assumed that a vehicle arrives at the mode arrival time and departs at the mode departure time. It is also assumed that the battery capacity corresponds to the expected value $\mu_{Bat} = 61.5\,\mathrm{kWh}$ (based on own calculation from data according to [36,37]) and the SoC corresponds to the expected value $\mu_{SoC} = 0.62$ (based on [38]). Only when an EV arrives are the real SoC and capacity used and the stay time is estimated based on the arrival time.

The linear optimisation balance model is shown in Fig. 7. The AIC feeds the DC grid from the AC grid and can either feed in or feed out. The EVs are connected to the DC grid via the charging infrastructure and can be charged or discharged. The stationary storage system can both charge to absorb energy from the DC grid and discharge to release energy to the grid. All other grid participants are summarised in the prosumer entity. The balance model is set up for all time steps $t \in T_{hor}$, which applies to all the following equations. For the DC grid (blue balancing group), the power balance of all incoming and outgoing power flows is calculated as

$$P^{var}_{AIC,in,t} - P^{var}_{AIC,out,t} + P^{var,}_{EV,Discharge,t} - P^{var}_{EV,Charge,t} - P^{var}_{ESS,t} = P^{*}_{Load,t} - P^{*}_{PV,t}. \quad (2)$$

$P^{*}_{PV,t}$ and $P^{*}_{Load,t}$ are predicted processes whose realisations are designated as $P_{PV,t}$ and $P_{Load,t}$. In contrast, all other outputs $P^{var}_{j,t}$ are optimisation variables under the boundary conditions

$$0 \le P^{var}_{AIC,in,t} \le P_{AIC,max} \quad (3)$$

$$0 \le P^{var}_{AIC,out,t} \le -P_{AIC,min} \quad (4)$$

$$0 \le P^{var}_{EV,Charge,t} \le P_{EV,max,t} \quad (5)$$

$$0 \le P^{var}_{EV,Discharge,t} \le -P_{EV,min,t} \quad (6)$$

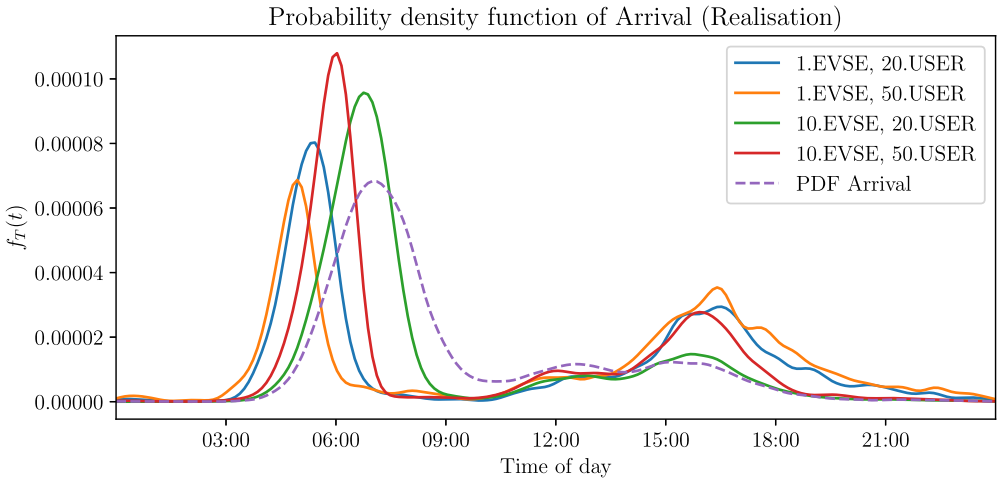

Fig. 5. Probability density function of arrival for different realised charging parks and different user volumes.

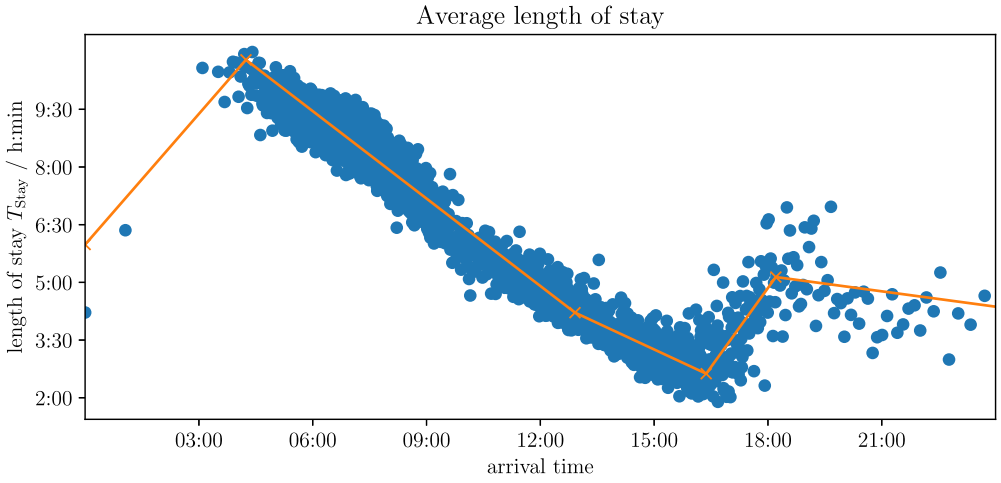

Fig. 6. Piecewise linear interpolation of the stay time over the arrival time of an EV at a charging station for 1 million realised arrivals.

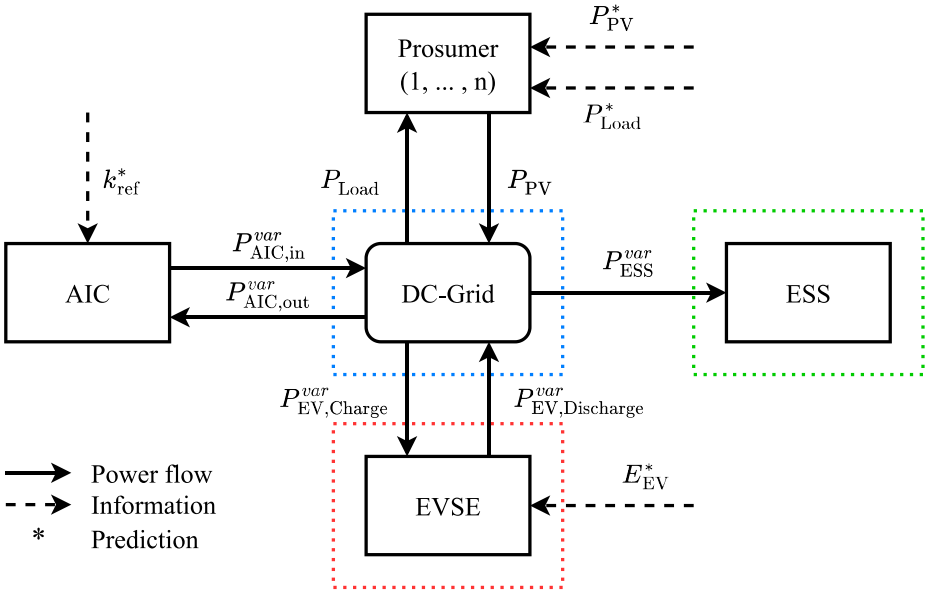

Fig. 7. Schematic representation of the balance model of a DC grid.

$$P_{\mathrm{ESS,min}} \leq P^{var}_{\mathrm{ESS,t}} \leq P_{\mathrm{ESS,max}}. \tag{7}$$

Unlike the power balance in the DC grid, the stationary storage system (green) and the EVs (red) are energy balances. For the ESS, the energy balance results in

$$E^{var}_{\mathrm{ESS,t}} = E^{var}_{\mathrm{ESS,t-1}} \cdot \eta_{\mathrm{ESS,T_{step}}} + P^{var}_{\mathrm{ESS,t}} \cdot T_{\mathrm{step}}, \tag{8}$$

where $\eta_{\mathrm{ESS,T_{step}}}$ is the efficiency of energy storage over time. The ESS is subject to the constraint

$$E_{\mathrm{ESS,min}} \leq E^{var}_{\mathrm{ESS,t}} \leq E_{\mathrm{ESS,max}}. \tag{9}$$

The energy balance of the predicted or connected EV results in

$$E^{var}_{\mathrm{EV,t}} = E^{var}_{\mathrm{EV,t-1}} + P^{var}_{\mathrm{EV,Charge,t}} \cdot T_{\mathrm{step}} - P^{var}_{\mathrm{EV,Discharge,t}} \cdot T_{\mathrm{step}}, \tag{10}$$

subject to the constraint

$$0 \leq E^{var}_{\mathrm{EV,t}} \leq E_{\mathrm{EV,max,t}}. \tag{11}$$

As long as no EV is connected, the predicted battery capacity E^{*}_{EV} is used for the maximum capacity. In this case, it is a multi-dimensional equation in which all energy balances of the n_{EVSE} charging stations are summarised. The energy balance corresponding to the connected battery capacity must be maintained for each EVSE. This EV battery storage model is a simplified linear battery model that does not take certain aspects into account. It is merely an electrical model that does not consider thermal aspects or battery degradation. However, this assumption is sufficient for the optimisation model used here, as the focus is solely on the electrical part. Furthermore, for the short period of one day, it can be assumed that temperature changes are minor and the thermal effects are minimal. The same applies to battery ageing. Short time horizons are considered in which no excessive battery use is expected. Furthermore, *Sagaria et al.* [39] were able to show in their study that the effects of V2G on battery ageing are very low compared to other factors. Similar findings were shown in a study by RWTH Aachen University [40].

The aim is to minimise the predicted CO_2 emissions as a grid-based reference value $k^{*}_{\mathrm{ref}} = m^{*}_{\mathrm{CO_2}}$. At the same time, the EV batteries should be charged by the predicted departure time at the latest. The objective function results in

$$\begin{aligned}\min \Bigg(& \sum_{t} (P^{var}_{\mathrm{AIC,in,t}} \cdot T_{\mathrm{step}} \cdot m^{*}_{\mathrm{CO_2,t}}) \\ & + \sum_{t} (P^{+}_{\mathrm{AIC,penalty,t}} \cdot T_{\mathrm{step}} \cdot 10 \cdot \hat{m}^{*}_{\mathrm{CO_2}}) \\ & + \sum_{i=0}^{n_{\mathrm{EVSE}}} (E_{\mathrm{EV,i,max}} - E^{var}_{\mathrm{EV,i,t_{disconnect}}}) \cdot \hat{m}^{*}_{\mathrm{CO_2}} \Bigg).\end{aligned} \tag{12}$$

The emissions of all time steps are summarised. In addition, the energy difference between the maximum energy in the EV's storage and the energy at the time of departure is assigned the maximum value of the emissions in the time horizon, so that it is always more favourable to charge than not to charge. Since load profiles and reference variables do not necessarily have to follow the predicted curve and droop control characteristics have an influence on the states in the DC grid, unrealisable start parameters may occur. Since solvability should be guaranteed, a positive virtual penalty $P^{+}_{\mathrm{AIC,penalty}}$ is inserted for this case.

Additional constraints ensure that there is no simultaneous feed-in and feed-out via the AIC. In addition, simultaneous charging and discharging of different electric vehicles should be prevented. This is based on the consideration that there should be no cross-charging from one EV to another. Before an EV has to be discharged to ensure grid stability or to just reduce the load, all other EVs should stop charging. If there is sufficient energy available to charge EVs, others do not need to be discharged. Binary variables can be used to resolve simultaneity. To ensure that the AIC is either feeding in or feeding out, the inequalities

$$P^{var}_{\mathrm{AIC,in,t}} \leq \delta^{var}_{\mathrm{AIC,t}} \cdot P_{\mathrm{AIC,max}} \tag{13}$$

$$P^{var}_{\mathrm{AIC,out,t}} \leq -(1 - \delta^{var}_{\mathrm{AIC,t}}) \cdot P_{\mathrm{AIC,min}} \tag{14}$$

are used. If $\delta^{var}_{\mathrm{AIC,t}} = 0$, there can be no feed-in to the DC grid. At the same time, the feed-out according to Eq. (14) can be less than or equal to $-P_{\mathrm{AIC,min}}$. A similar procedure is used for charging and discharging the EV. The binary variable $\delta^{var}_{\mathrm{EV,t}}$ is used to ensure that the EV is either charging or discharging. However, this also removes the possibility of one EV being discharged and another being charged at the same time. This is realised by the inequalities

$$P^{var}_{\mathrm{EV,Charge,t}} \leq \delta^{var}_{\mathrm{EV,t}} \cdot P_{\mathrm{EV,max}} \tag{15}$$

$$P^{var}_{\mathrm{EV,Discharge,t}} \leq -(1 - \delta^{var}_{\mathrm{EV,t}}) \cdot P_{\mathrm{EV,min}}. \tag{16}$$

If the binary variable $\delta^{var}_{\mathrm{EV,t}} = 1$, the EVs are charged, while they are discharged if $\delta^{var}_{\mathrm{EV,t}} = 0$.

Binary variables are also used to indicate special states of the optimisation. For this purpose, constraints are extended by a sufficiently large number M (*Big-M*), whereby intervals of the optimisation variables are limited to M. The use of the variable M represents an upper or lower bound for the respective optimisation variable [41]. The inequalities

$$P^{var}_{\mathrm{AIC,in,t}} \leq P_{\mathrm{AIC,max}} + M \cdot \delta^{var}_{\mathrm{AIC,max,t}} \tag{17}$$

$$P^{var}_{\mathrm{AIC,in,t}} \geq P_{\mathrm{AIC,max}} - M \cdot (1 - \delta^{var}_{\mathrm{AIC,max,t}}), \tag{18}$$

with $M = P_{\mathrm{AIC,max}}$ ensure that $\delta^{var}_{\mathrm{AIC,max,t}}$ can only be equal to one if $P^{var}_{\mathrm{AIC,in,t}} = P_{\mathrm{AIC,max}}$. For $\delta^{var}_{\mathrm{AIC,max,t}} = 0$, $P^{var}_{\mathrm{AIC,in,t}}$ can lie in the interval $[0, P_{\mathrm{AIC,max}}]$. This does not mean that for $\delta^{var}_{\mathrm{AIC,max,t}} = 0$ at the same time $P^{var}_{\mathrm{AIC,in,t}} \neq P_{\mathrm{AIC,max}}$. In fact, the optimisation variable $\delta^{var}_{\mathrm{AIC,max,t}}$ can only be equal to one if $P^{var}_{\mathrm{AIC,in,t}} = P_{\mathrm{AIC,max}}$. The same procedure is used for the ESS, so that

$$P^{var}_{\mathrm{ESS,t}} \geq P_{\mathrm{ESS,min}} + M \cdot \delta^{var}_{\mathrm{ESS,min,t}} \tag{19}$$

$$P^{var}_{\mathrm{ESS,t}} \leq P_{\mathrm{ESS,min}} - M \cdot (1 - \delta^{var}_{\mathrm{ESS,min,t}}) \tag{20}$$

and $M = P_{\mathrm{ESS,min}} - P_{\mathrm{ESS,max}}$ can be used to determine whether the power $P^{var}_{\mathrm{ESS,t}}$ of the ESS is minimal. $\delta^{var}_{\mathrm{ESS,min,t}}$ can only be equal to one if the power is minimal and therefore the ESS feeds into the DC grid as much as possible. In addition

$$E^{var}_{\mathrm{ESS,t}} \leq E_{\mathrm{ESS,low}} + M \cdot (1 - \delta^{var}_{\mathrm{ESS,SoC,t}}) \tag{21}$$

$$E^{var}_{\mathrm{ESS,t}} \geq E_{\mathrm{ESS,low}} - M \cdot \delta^{var}_{\mathrm{ESS,SoC,t}} \tag{22}$$

and $M = E_{\mathrm{ESS,max}}$ can be used to determine whether the SoC of the ESS is below or above a threshold $E_{\mathrm{ESS,low}} \in [E_{\mathrm{ESS,min}}, E_{\mathrm{ESS,max}}]$. Above is $\delta^{var}_{\mathrm{ESS,SoC,t}} = 0$ and below is $\delta^{var}_{\mathrm{ESS,SoC,t}} = 1$. Similarly, the binary variables $\delta^{var}_{\mathrm{EV,min,t}}$ and $\delta^{var}_{\mathrm{EV,SoC,t}}$ result via the inequalities

$$P^{var}_{\mathrm{EV,Discharge,t}} \leq -P_{\mathrm{EV,min,t}} + M \cdot \delta^{var}_{\mathrm{EV,min,t}} \tag{23}$$

$$P^{var}_{\mathrm{EV,Discharge,t}} \leq -P_{\mathrm{EV,min,t}} - M \cdot (1 - \delta^{var}_{\mathrm{EV,min,t}}) \tag{24}$$

$$\text{with } M = -P_{\mathrm{EV,min,t}} \tag{25}$$

and

$$E^{var}_{\mathrm{EV,t}} \leq E_{\mathrm{EV,low,t}} + M \cdot (1 - \delta^{var}_{\mathrm{EV,SoC,t}}) \tag{26}$$

$$E^{var}_{\mathrm{EV,t}} \geq E_{\mathrm{EV,low,t}} - M \cdot \delta^{var}_{\mathrm{EV,SoC,t}} \tag{27}$$

$$\text{with } M = E_{\mathrm{EV,max,t}}. \tag{28}$$

$\delta^{var}_{\mathrm{EV,min,t}} = 1$ is only possible if the EV discharges at maximum power, while for $\delta^{var}_{\mathrm{EV,SoC,t}} = 1$ the SoC must fall below the threshold $E_{\mathrm{EV,low,t}}$.

By linking these different binary optimisation variables, permitted states can be specifically controlled or linked to each other. For this purpose, it is sometimes necessary to introduce additional binary variables as helper variables, which are linked to each other by logical operators. The binary variables are used here to allow the penalty power only if the AIC feeds in with maximum power and the SoC of the ESS is below the minimum threshold. In addition, the penalty power cannot be used if EVs are charging at the same time. Furthermore,

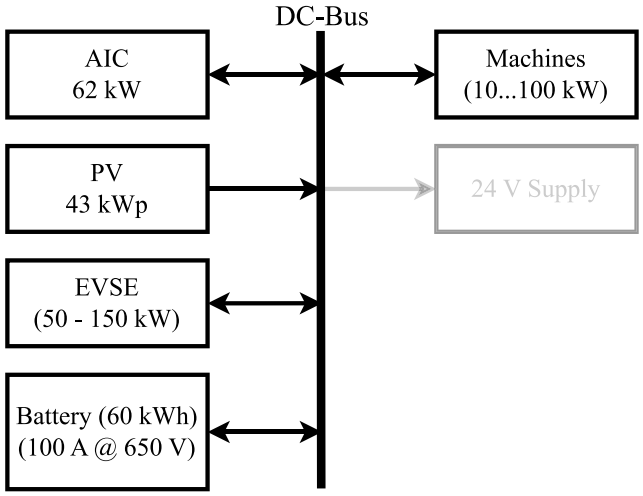

Fig. 8. Structure of the DC grid of the test facility.

the EVs must also feed in with maximum power into the DC grid in this case. Binary variables are used to ensure the mobility needs of EV users are met while maintaining EV reserves. This ensures that EVs are only discharged when the AIC is feeding into the DC grid at maximum power. This prevents the energy from the EVs from being used exclusively for the DC grid. It also enables the EVs to be charged without specifying a target SoC. The aim is to meet the mobility needs of users while allowing degrees of freedom in the optimisation. In addition, an attempt is made to meet the mobility requirements of users by predicting their stay time (compare Fig. 6).

If an optimal solution minimising the objective function while meeting all constraints is found, the results $P^{opt}_{\mathrm{AIC,in,t}}$, $P^{opt}_{\mathrm{AIC,out,t}}$, $P^{opt}_{\mathrm{EV,Charge,t}}$, $P^{opt}_{\mathrm{EV,Discharge,t}}$ and $P^{opt}_{\mathrm{ESS,t}}$ serve as the optimal setpoints for active participants. These are applied by adjusting the droop control characteristics in the DC grid. The sequential optimisation is repeated every T_{exec} over the horizon T_{hor}, but only the first m steps are used as the EMS output and setpoints $\vec{P}_{\mathrm{opt}}$. The output is summarised in the vector

$$\vec{P}_{\mathrm{opt}} = \begin{pmatrix} P^{opt}_{\mathrm{AIC,in,t}} \\ P^{opt}_{\mathrm{AIC,out,t}} \\ P^{opt}_{\mathrm{EV,Charge,t}} \\ P^{opt}_{\mathrm{EV,Discharge,t}} \\ P^{opt}_{\mathrm{ESS,t}} \end{pmatrix} \quad \text{with} \quad t \in mT_{\mathrm{step}}. \tag{29}$$

2.3. Case study of a DC grid in a test facility

The development of a specific EMS for DC grids requires a specific application. The DC grid of a test facility therefore serves as a case study. A schematic structure of the test facility is shown in Fig. 8. It comprises machines (10 kW to 100 kW), 24 V peripheral devices, a 43 kW PV system, a stationary battery storage system, bidirectional charging points and an 62 kW AIC. Droop control characteristics are implemented for the active participants, while all loads present are summarised in a load profile. In addition to the AIC and the ESS, a droop control characteristic is implemented for the PV system. The mathematical equations are given in the Appendix B. The overall characteristic curve for the use case is shown in red in Fig. 9 and results from the addition of the individual droop curves. The load profile of the machines and devices is generated synthetically. It is based on the assumption of a base load in the form of the scaled standard load profile G0 [42], which is used in the prediction. The base load is overlaid with a variable load in the form of a *random walk* between ±15 kW and a white noise with the expected value $\mu_{\mathrm{P,var}} = 0\,\mathrm{kW}$ and the standard deviation $\sigma_{\mathrm{P,var}} = 1\,\mathrm{kW}$. This creates the load profile shown in Fig. 10 with the standard load profile G0 as the load prediction.

The scenarios at the charging stations are generated synthetically. For $n_{\mathrm{EVSE}} = 4$ charging stations and a daily user volume of $n_{\mathrm{User}} = 20$ EVSE arrivals, scenarios such as those shown in Fig. 11 result. During the day from 06:00 to 18:00, all charging points are usually occupied, while they are typically not occupied during the night. This is a logical assumption, as more users want to use the EVSE than there are stations available. Since there is no obligation to leave the EVSE once an EV is charged and no maximum time limit for occupying a charging station, there is little fluctuation. If there were more EVSE available than EVs intending to charge, or if user traffic were lower, not all EVSE would be occupied and there would be even less fluctuation. Therefore, on average, the largest mobile storage capacity is available during the day. Based on the mode arrival and departure time and the expected value of the battery capacity and the SoC, the availability of the EV capacity can be predicted. This prediction is shown in the upper part of Fig. 12. As soon as an EV is connected to an EVSE, the current SoC and the maximum capacity are known. The average stay time can now be estimated based on the arrival time (see Fig. 6). In the lower part of Fig. 12, this is shown in orange for the example scenario from Fig. 11. The figure shows that the prediction is a good approximation for both unused and occupied EVSEs and can therefore be used by an EMS. This looks similar in other scenarios. On average, this results in a good prediction, even if individual deviations are sometimes considerable. The accuracy increases with the number of charging stations, as deviations are averaged out. Individual predictions are not more accurate.

3. Results

3.1. Energy management in industrial DC grids

A comparison with an unmanaged system is required in order to analyse different EMS. Simulations show that unmanaged charging causes peak loads. In the DC grid, the ESS discharges first, which means that it can no longer provide energy later. This leads to increased AIC power and fluctuating energy consumption. In addition, the ESS is recharged with a delay due to the high load. The simulation of the fuzzy logic EMS (Fig. 13) shows high constant power levels of the AIC in some cases. The ESS charges quickly to above 75 % SoC and remains there. The EVSE power drops by 50 %, which means that EVs charge more slowly. When the SoC in the bottom subfigure drops to zero, this indicates that one EV disconnects from the EVSE, allowing another EV to be connected. If no EV is connected to an EVSE, the SoC is set to zero. EVs connected for a short time may not fully reach their target SoC. Nevertheless, all EVs reach at least 95 % SoC. The maximum AIC power decreases from 76 kW to 38 kW, the average remains at about 32 kW. In contrast to a fuzzy logic EMS, an EMS with sequential linear optimisation acts predictive. Predictions and *a priori* provided setpoint states allow energy flows to be controlled in a specific way. Each optimisation takes into account the current system states and adjusts the setpoints. Unforeseen events are processed by droop control characteristics, while the resulting states serve as starting values for the next optimisation. The decisive factors are the execution interval T_{exec}, the step size T_{step} and the prediction horizon T_{hor}. The investigation of different horizons has shown that a time horizon of 24 h delivers the best results. The step size of the optimisation is set to $T_{\mathrm{step}} = 5\,\mathrm{min}$ and repeated at a $T_{\mathrm{exec}} = 15\,\mathrm{min}$ interval.

For the daily simulation, the PV power prediction is required to determine the residual load and the reference variable k^*_{ref} to minimise the objective function. The PV prediction is assumed to be faultless, while the CO_2 emissions in the electricity mix are calculated in prior and not adjusted. The optimisation is performed sequentially, whereby only the first optimisation time step $P_{opt}(t_0)$ with duration T_{step} is implemented. This is adjusted via droop control characteristics until

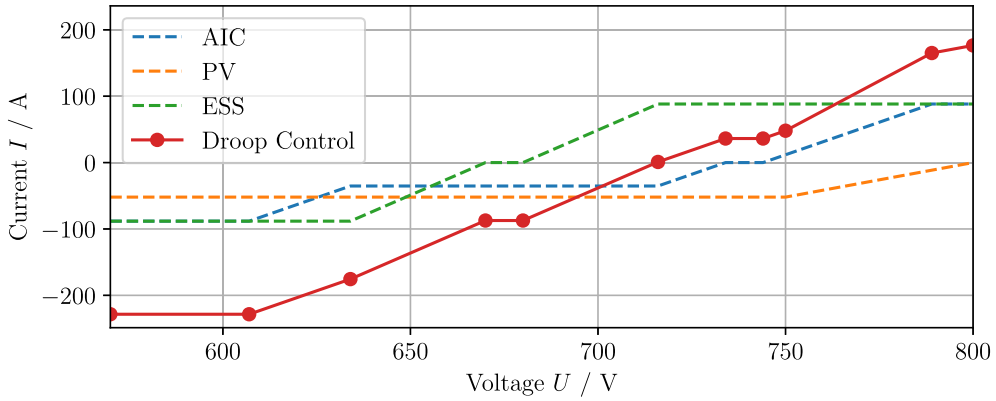

Fig. 9. Implemented droop control curves of the DC grid of the test facility.

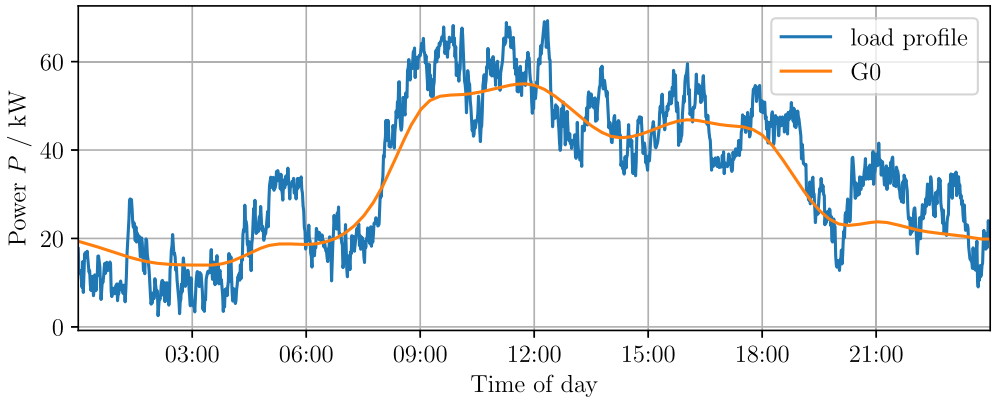

Fig. 10. Synthetic load profile and standard load profile G0 [42].

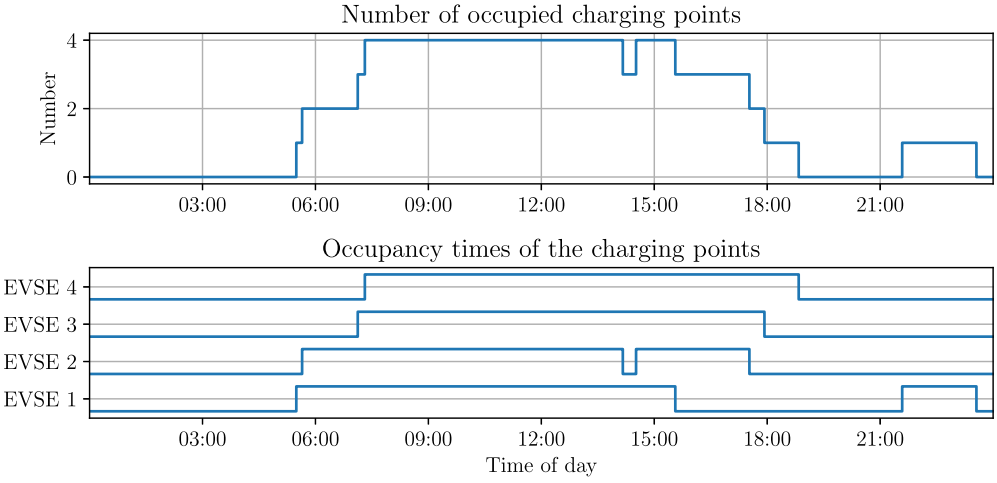

Fig. 11. Number of occupied charging points and occupancy times of an example scenario of a charging park with four charging stations. The charging point is free at zero and occupied at one.

the next optimisation. The setpoint curve results from the sequence of these steps. Minor deviations between prediction and real load improve accuracy. More precise load and EV availability predictions further optimise the result. It was shown that the prediction of CO_2 emissions enable grid-friendly operation.

Fig. 14 shows the simulation results with setpoint specifications. The top diagram shows the DC grid voltage, followed by the power and setpoint power of the participants AIC, ESS and the charging stations. The SoC of the ESS is marked in green, followed by the SoCs of the EVs at the respective EVSE. The AIC power $P_{\mathrm{AIC,act}}$ almost corresponds to the setpoint power $P_{\mathrm{AIC,set}}$, with exceptions at 04:00 and 09:00, when the ESS is discharged and cannot compensate for load fluctuations. This causes the DC grid voltage to drop until the AIC power increases according to the droop control characteristic (see Fig. 9). As soon as the ESS reaches a minimum SoC, the AIC follows the setpoint again and load fluctuations are equalised by P_{ESS}.

Fig. 14 shows also that the ESS is actively used, recognisable by the SoC fluctuation between 0 % and 100 %. The difference between

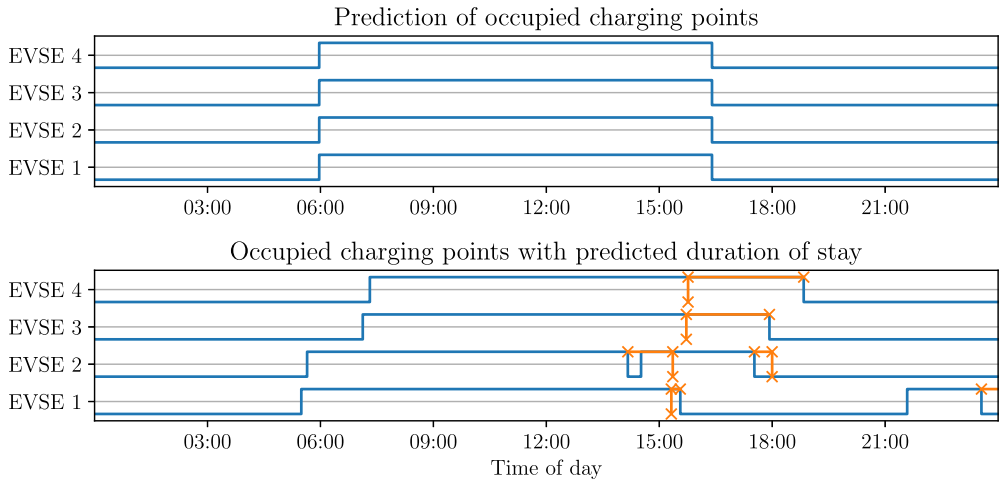

Fig. 12. Prediction of the occupancy times of a charging park with four charging stations when no EV is connected (top) and prediction of the stay time as soon as an EV is connected (bottom).

maximum and minimum AIC power is greater than with fuzzy logic, while the power curve remains more stable. The SoCs of the EVs show a load shift for grid-friendly behaviour. In contrast to fuzzy logic, vehicles are not charged immediately with reduced power, but charging is shifted to more favourable periods. The EVSE power output P_{EVSE} always remains below the setpoint power $P_{\mathrm{EV,set}}$ requested by the EVs and the setpoint power of the charging stations $P_{\mathrm{EVSE,set}}$. The optimisation is based on the maximum available power per charging station, not on the setpoint power of the EV, so that the limitation takes place within the charging station. At around 09:00, it becomes apparent that the ESS is discharged and the AIC target power is not sufficient. Due to the falling DC grid voltage, the EVs are briefly discharged via the droop control characteristics.

3.2. Analysis of grid-serving behaviour of simulation results

To assess the effects of the two EMSs used, the GSC is calculated over 24 h (see Section 2.2.1). An unmanaged charging of the EVs, in combination with the combined machine load (see Fig. 10), results in a GSC value of $GSC^{24\,\mathrm{h}}_{\mathrm{CO_2,noEMS}} = 0,987$. In contrast the EMS based on fuzzy logic ($GSC^{24\,\mathrm{h}}_{\mathrm{CO_2,Fuzzy}} = 0,991$) results in a slightly higher GSC, most likely due to an excessively high offset current, which increases the AIC power and utilises the ESS less.

Only in isolated simulations was it possible to achieve lower GSC values with fuzzy logic EMS than without an EMS. This was particularly the case when the total load in the DC grid did not inherently result in a constant residual load. This is based on the assumption that a constant load is, by definition, assigned a $GSC = 1$ and that a change towards a constant load can also be an improvement. In general, however, fuzzy logic did not achieve any improvement towards a constant residual load. A sequential optimised EMS achieves an approximately 7% better grid-serving behaviour ($GSC^{24\,\mathrm{h}}_{\mathrm{CO_2,Opt}} = 0,923$) as it enables load shifting and more intensive ESS use. This is shown by the total cumulative amount of energy exchanged between the grid and the storage system: $E_{\mathrm{cum,Fuzzy}} = 103\,\mathrm{kW\,h}$ vs $E_{\mathrm{cum,Opt}} = 279\,\mathrm{kW\,h}$. Another criterion is the CO_2 emissions from energy procurement. For comparability, the difference between final SoC and full charge of the ESS and the EV is evaluated with the average daily emissions. The absolute CO_2 emission is $m_{\mathrm{CO_2,Fuzzy}} = 294\,\mathrm{kg}$ and $m_{\mathrm{CO_2,Opt}} = 253\,\mathrm{kg}$. As the emissions are lower with sequential optimisation, this indicates better results, due to gird-serving behaviour is determined based on the emissions. Since no significant positive effects could be demonstrated through the use of fuzzy logic, the following focuses on analysing the effects of sequential optimisation.

The GSC was analysed under variable load, different maximum AIC power and different ESS capacities. For this purpose, scaled load profiles (60 %, 80 %, 100 %), ten random EV charging scenarios and four days with different PV power are simulated. Fig. 15 shows that the load variation has barely any influence on the GSC. Surprisingly, a higher load sometimes led to better GSC values. Scenarios 2 and 9 deviate more strongly, as here many vehicles are charged between 15:00 and 18:00 with a short duration of stay. As the CO_2 emissions are high during this period (even maximum on 21 March), the GSC decreases. Fig. 16 shows that a higher AIC power or greater ESS capacity usually improves the GSC represented grid-serving behaviour. Exceptions are scenarios 3 and 9, where $P_{\mathrm{AIC,max}} = 80\,\mathrm{kW}$ is more grid-friendly than $P_{\mathrm{AIC,max}} = 100\,\mathrm{kW}$. Larger storage capacities are always more favourable, presumably due to higher available power and better load shifting potential.

3.3. Transient stability analysis of various failure scenarios

Analysing failures of active devices allows them to be classified as non-critical, potentially critical and critical. A load drop, for example due to an emergency shutdown, is considered non-critical as the feed-in is immediately reduced via the droop control characteristics. Two scenarios were simulated: A load drop to 30 % for 30 and 60 min respectively. During the drop, the voltage increases, causing the ESS to absorb energy. When it is fully charged, the AIC reduces the power. As the AIC typically feeds into the grid, the load reduction is not critical.

If the AIC fails without falling energy demand, this leads to a voltage drop in the DC grid. Simulations have shown that the ESS discharges immediately until it is empty, whereupon the voltage drops further. The EVs then take over the provision of power through bidirectional feedback, but with limited power. As soon as the ESS is discharged, the EVSE power becomes negative. A low SoC of the EV or longer outages could jeopardise grid stability. Bridging is therefore only possible to a limited extent, and the AIC failure is considered critical.

The ESS failure is classified as potentially critical, as the AIC can increase the energy feed-in via the droop control characteristic. Simulations have shown that other participants take over the ESS function. The AIC in particular can take over the provision of power and compensate for load fluctuations. This results in greater voltage fluctuations, as the grid voltage must first deviate below 634 V or above 716 V before the AIC reacts. There was no recognisable influence on the EV charging processes as the AIC takes over the feed-in.

The situation is similar in the event of a charging infrastructure failure, with the difference that the ESS absorbs the energy before the AIC reduces the power. A failure of the charging infrastructure

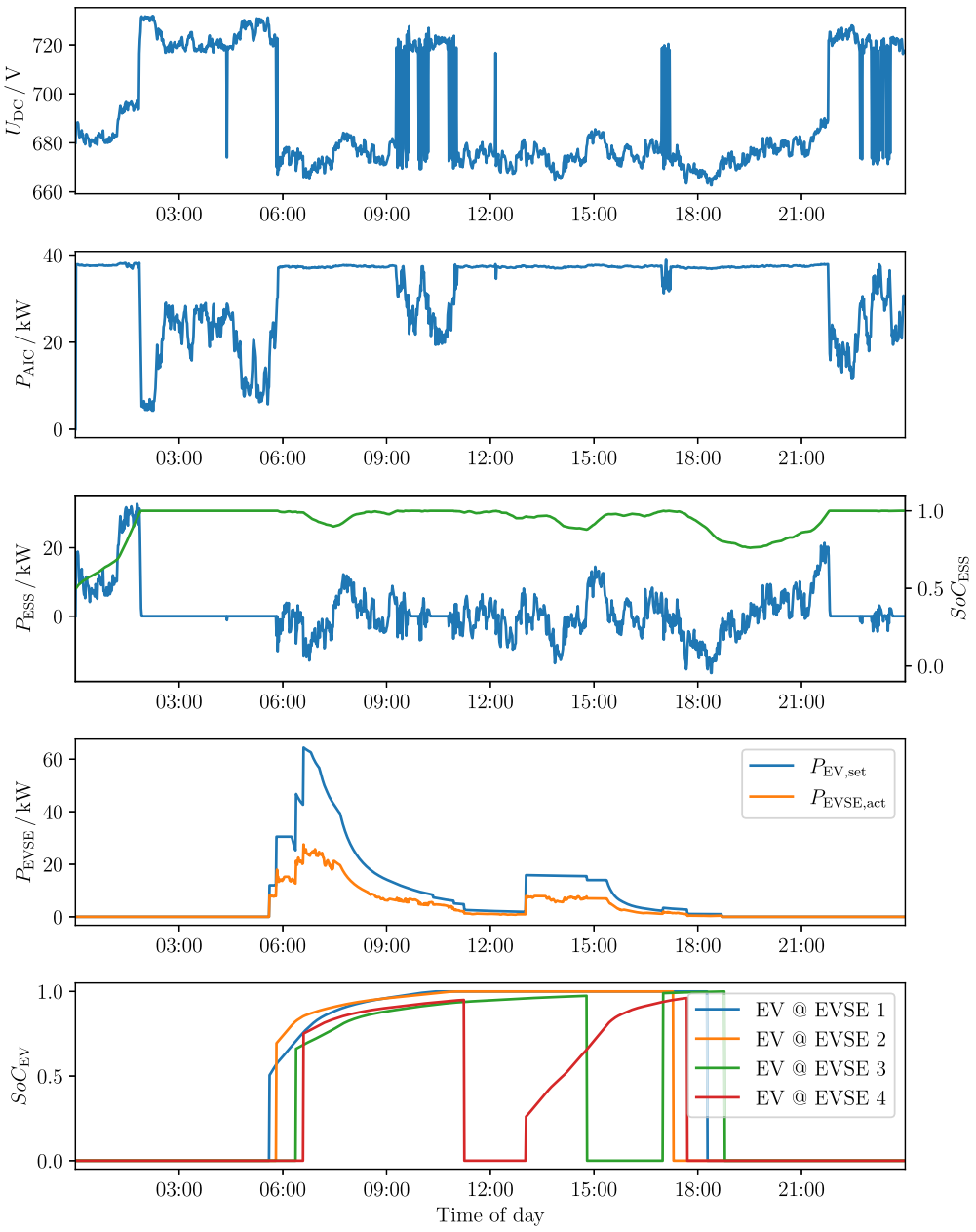

Fig. 13. Simulation result of a DC grid simulation of one day with an EMS based on fuzzy logic.

is categorised as non-critical, as is a drop in load. In a simulation, it was shown that the failure of the charging infrastructure provides energy, which primarily charges the ESS. A failure of the charging infrastructure therefore only ensures that the charging of the EV is delayed.

4. Discussion

In this section, the simulation results are discussed and critically analysed, with particular attention paid to specific characteristics of the results.

It should be noted that DC grids can be used via EMS to ensure grid-serving behaviour by load shifting and aligning load with renewable generation towards higher-level AC grids. This applies to an optimised EMS, whereas a purely rule based fuzzy EMS is only suitable to a limited extent. Its advantage lies in its easier implementation. However, a pronounced positive effect on grid-serving behaviour, represented by the GSC could not be determined. Nevertheless, a lower peak load was achieved, with low emissions at the same time.

It has been demonstrated that an EMS based on sequential MILP optimisation can improve grid-serving behaviour through demand side management. The specific CO_2 emissions of the electricity mix were used for this purpose, as it has been shown that these correlates particularly well with residual load and can be predicted based on weather forecasts. The significance of the indicator used, which is only calculated for one day, must be critically questioned. A differentiated analysis of this issue could be useful for future research and could be compared with the results of this study. It should also be noted that the use of an EMS increases the difference between the minimum and maximum power of the grid interconnection point. Regarding the AC grid and potential grid overloads, it must be investigated whether these fluctuations have a negative effect. This is not mapped via the grid support coefficient.

Furthermore, conflicting objectives must be analysed. For example, any grid-serving behaviour like peak clipping or load shifting could

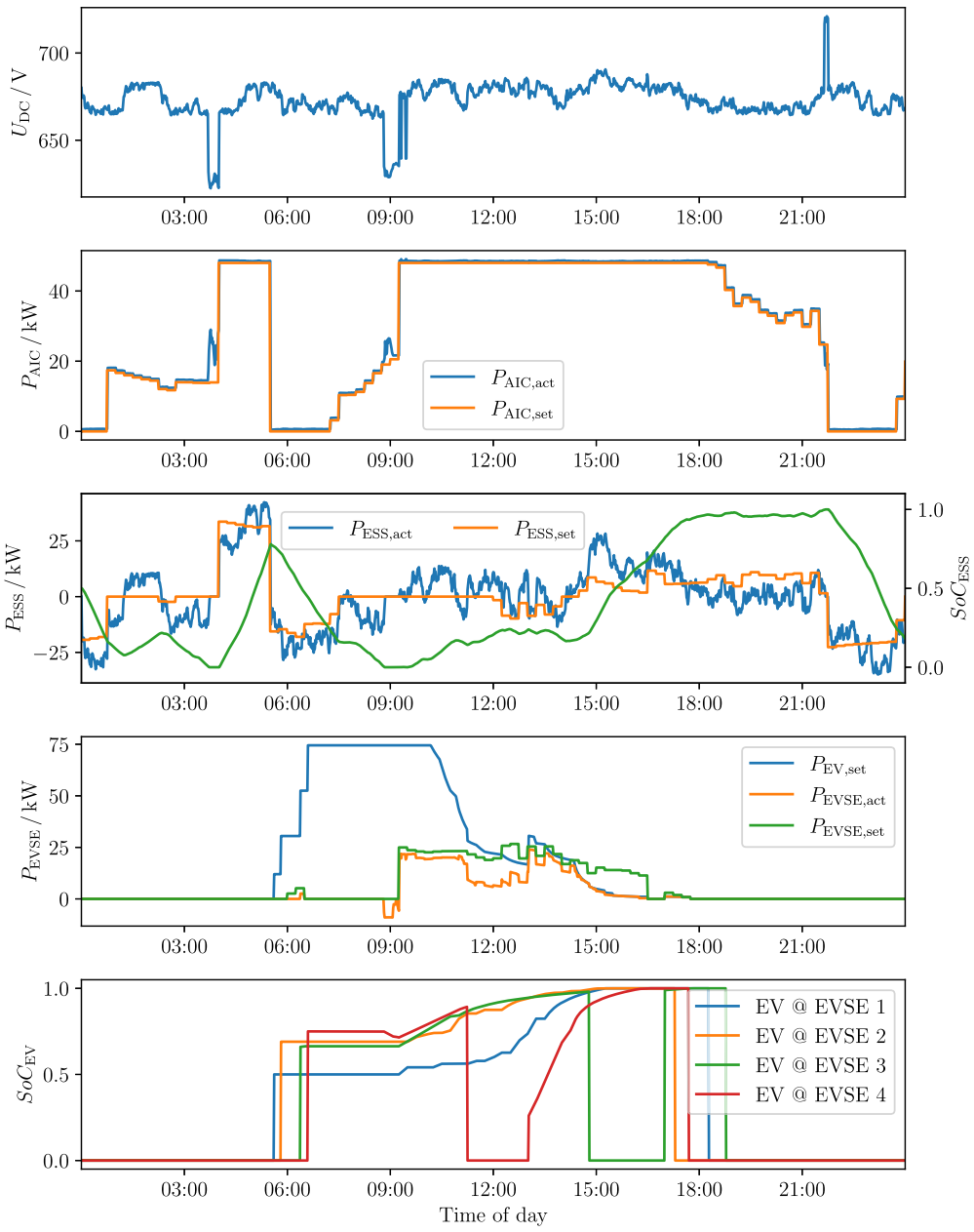

Fig. 14. Simulation result of a DC grid simulation of one day with an EMS based on sequential optimisation.

have an unpredictable impact on electricity prices if many market participants act in this way, which was not examined in this study. Different objectives must also be considered when establishing an EMS in industrial DC grids. If the objective is exclusively to charge EVs, the objective cannot be to support the DC grid with energy from EVs or to act exclusively in a grid-serving manner. This paper examined the impact of bidirectional charging in DC grids on higher-level AC grids in terms of GSC represented grid-serving behaviour. It has been shown that the ability to charge EVs bidirectionally is only used to a negligible extent when the goal is to ensure individual mobility. A comparison with other charging strategies is pending, as further issues such as battery ageing, which has been neglected here, could be incorporated.

Typically, grid-serving behaviour is achieved by load shifting the charging processes. It remains to be clarified whether EVs should feed energy back into the AC supply grid in the future to improve AC grid stability by providing extra flexibility, or whether they should only feed back into the DC grid. The latter approach is more interesting for highly cyclical or peak load-dominated industrial applications, such as welding robots or in cases where high starting currents from electric motors occur. In addition, apart from consumption-based indirect monetary compensation, there is currently neither a need nor an explicit incentive to intelligently connect the DC grid to the supply grid. For this reason, feeding into the DC grid remains dominant.

Finally, the limitations of the approach presented should be mentioned. The DC grid considered in this paper is rather small, with a feed-in capacity of 62 kW and four EVSEs, so the question must be asked whether the added value provided by demand side management also applies to grid services in significantly larger grids. Furthermore, this is an industrial DC grid that can be expanded with EVSEs. In other typical areas of application for DC grids, such as in marine electrical systems as in *Zemin et al.* [43], this option is not available, which limits the approach presented. Moreover, this approach only makes sense in AC-coupled DC grids, as only these can act as variable loads with the possibility to supply the AC grid. Another possibility could be DC grids

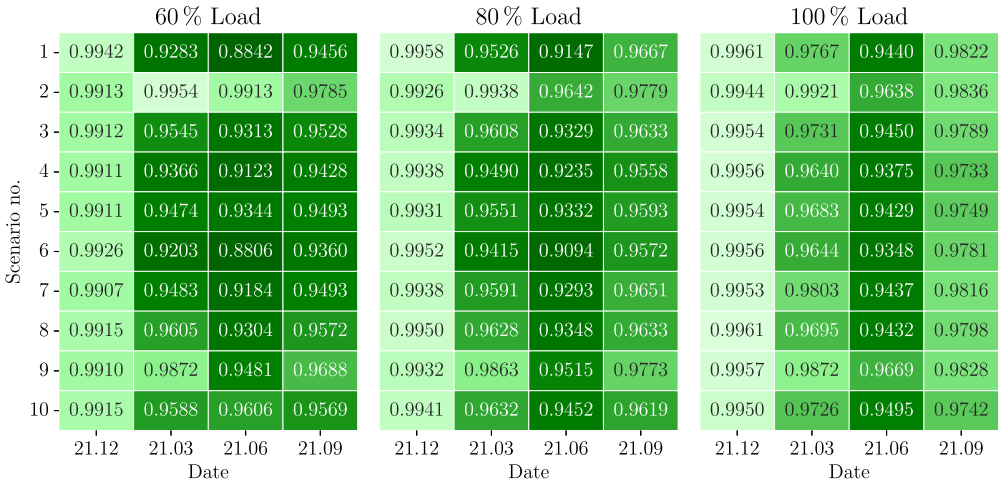

Fig. 15. Grid support coefficients for different scenarios and different days representing the PV output in different seasons, for three weighted load profiles.

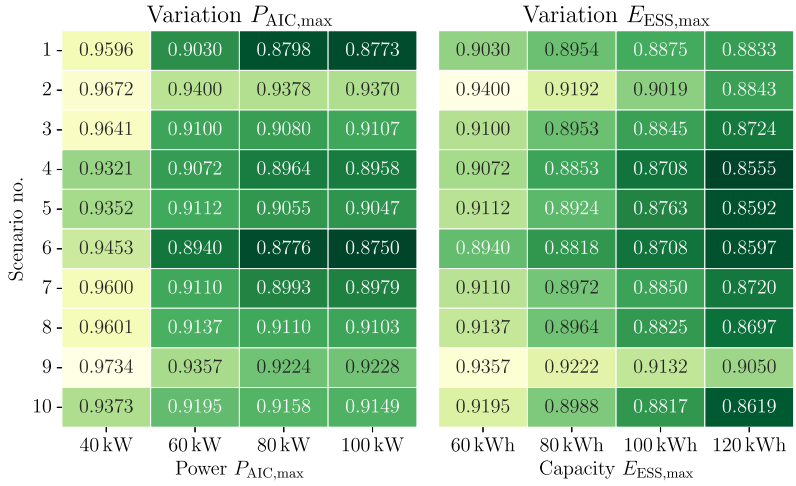

Fig. 16. Grid support coefficients for different scenarios and the variation of the maximum AIC power or the maximum capacity of the ESS.

in a non-industrial context, such as in neighbourhoods and residential complexes, for better utilisation and storage of renewable energy.

To utilise rolling time horizons, predictions are required that are associated with uncertainty. It should be discussed whether a stochastic approach can be used to counter this. This would require probability distributions to be incorporated into the optimisation process.

5. Conclusion

This paper presents a study of the grid-serving behaviour of an industrial DC grid equipped with a bidirectional charging infrastructure for EVs. For this purpose, a grid support coefficient and simulations in MATLAB® and Simulink® were used. A laboratory test facility serves as a case study, based on which two EMS were developed: a system based on fuzzy logic and an optimised system based on predictions. CO_2 emission forecasts were identified and used as reference variables, as it was demonstrated that they correlate with the residual load.

Both EMS were simulated over one day. It was shown that both systems can satisfy the mobility needs of EV users. At the same time, the implementation of MILP based sequential optimisation has resulted in improved coefficient represented grid-serving behaviour through load shifting. It was also shown that a load reduction has a smaller influence than the availability of PV energy. Furthermore, increasing the maximum power of the grid connection point and increasing the stationary storage capacity has a positive effect.

Critical scenarios for grid stability were identified by analysing various failure scenarios. It has been shown that the failure of the grid connection point jeopardises transient DC grid stability. A stationary storage system can only bridge outages to a certain extent, as either the maximum output is not sufficient, or the capacity is too low. Bidirectional charging stations provide a remedy, as they have the possibility to feed power back into the DC grid in critical situations.

The EMS proposed in this study demonstrated coefficient represented grid-serving behaviour by enabling bidirectional charging in DC grids. By applying an optimised EMS, the coefficient improved by 7%, while lowering the demand based emissions by 41 kg a day compared to fuzzy based EMS. In addition, the integration of EV storage capacity enhanced the security and reliability of the DC energy supply.

These results highlight that implementing bidirectional charging through an EMS provides tangible benefits for operators of industrial DC grids. Besides to the possibility of load shifting to minimise emissions, it is also possible to bridge AC grid connection failures, thereby increasing security of supply. At the same time, it is possible to act as a supportive load in relation to the AC grid. As well as load shifting, this is achieved by adjusting peak loads in favour of a more constant residual load. As it is likely that consumption behaviour adapted to AC grid conditions will become increasingly relevant, bidirectional charging should be considered when defining future operating strategies for DC grids.

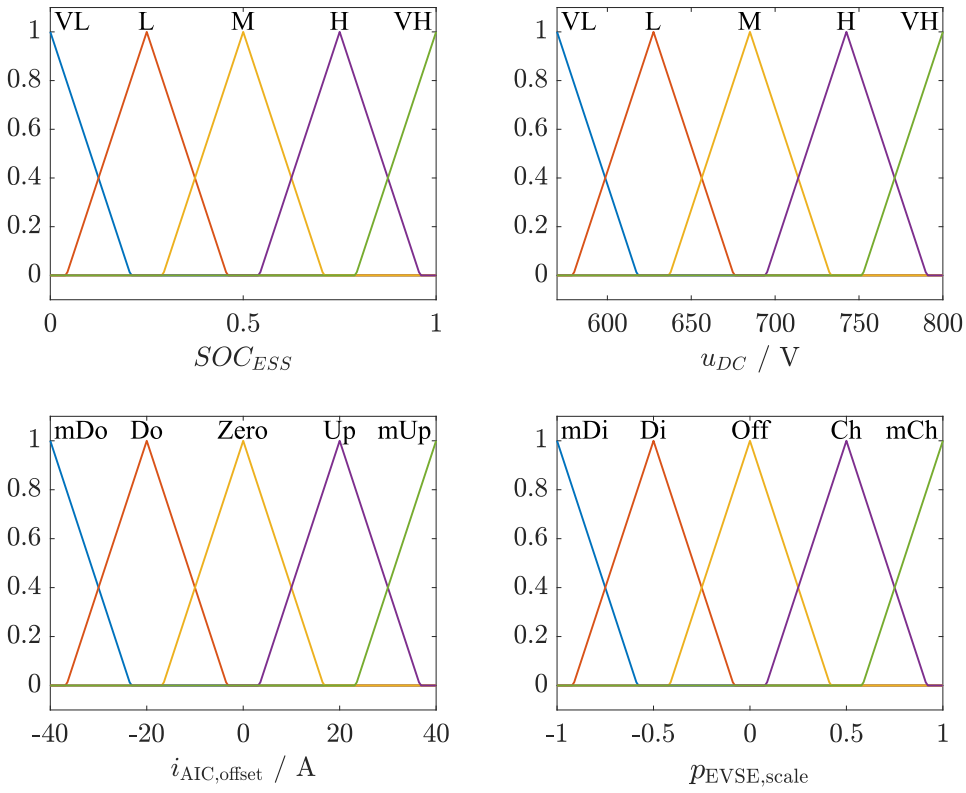

Fig. A.17. Membership functions of the inputs and outputs of fuzzy control.

CRediT authorship contribution statement

Henning Rahlf: Writing – review & editing, Writing – original draft, Visualization, Software, Resources, Methodology, Investigation, Formal analysis, Data curation, Conceptualization. **Lukas Knorr:** Writing – review & editing, Methodology, Formal analysis, Conceptualization. **Simon Althoff:** Writing – review & editing, Supervision, Project administration. **Henning Meschede:** Writing – review & editing, Supervision.

Use of AI-assisted technologies

During the preparation of this work the authors used ChatGPT-4 provided by OpenAI and DeepL provided by DeepL SE in order to improve sentence structure, grammar and spelling. After using these services, the authors reviewed and edited the content as needed and take full responsibility for the content of the publication.

Declaration of competing interest

The authors declare that they have no known competing financial interests or personal relationships that could have appeared to influence the work reported in this paper.

Acknowledgment

I acknowledge support for the publication cost by the Open Access Publication Fund of Paderborn University.

Appendix A. Fuzzy logic energy management system

Fig. A.17 presents the membership functions of the fuzzy logic inputs and outputs, while the associated rule base is given in Table A.1. These elements define the mapping from DC grid voltage and ESS SoC to the output variables $i_{\mathrm{AIC,offset}}$ and $p_{\mathrm{EVSE,scale}}$.

Appendix B. Droop control characteristics of the test facility

This section shows the mathematical equations of the piecewise linear droop control characteristics according to Fig. 9.

Active Infeed Converter (AIC):

$$I(U) = \begin{cases} -88\,\mathrm{A}, & 570\,\mathrm{V} \le U \le 607\,\mathrm{V} \\ 1.96\,\frac{\mathrm{A}}{\mathrm{V}} \cdot U - 1278\,\mathrm{A}, & 607\,\mathrm{V} < U < 634\,\mathrm{V} \\ -35\,\mathrm{A}, & 634\,\mathrm{V} \le U \le 716\,\mathrm{V} \\ 1.96\,\frac{\mathrm{A}}{\mathrm{V}} \cdot U - 1439\,\mathrm{A}, & 716\,\mathrm{V} < U < 734\,\mathrm{V} \\ 0\,\mathrm{A}, & 734\,\mathrm{V} \le U \le 744\,\mathrm{V} \\ 1.96\,\frac{\mathrm{A}}{\mathrm{V}} \cdot U - 1458\,\mathrm{A}, & 744\,\mathrm{V} < U < 789\,\mathrm{V} \\ 88\,\mathrm{A}, & 789\,\mathrm{V} \le U \le 800\,\mathrm{V} \\ 0\,\mathrm{A}, & else \end{cases} \tag{B.1}$$

Energy Storage System (ESS):

$$I(U) = \begin{cases} -88\,\mathrm{A}, & 570\,\mathrm{V} \le U \le 634\,\mathrm{V} \\ 2.45\,\frac{\mathrm{A}}{\mathrm{V}} \cdot U - 1642\,\mathrm{A}, & 634\,\mathrm{V} < U < 670\,\mathrm{V} \\ 0\,\mathrm{A}, & 670\,\mathrm{V} \le U \le 680\,\mathrm{V} \\ 2.45\,\frac{\mathrm{A}}{\mathrm{V}} \cdot U - 1667\,\mathrm{A}, & 680\,\mathrm{V} < U < 716\,\mathrm{V} \\ 88\,\mathrm{A}, & 716\,\mathrm{V} \le U \le 800\,\mathrm{V} \\ 0\,\mathrm{A}, & else \end{cases} \tag{B.2}$$

Photovoltaics (PV):

$$I(U) = \begin{cases} -52\,\mathrm{A}, & 570\,\mathrm{V} \le U \le 750\,\mathrm{V} \\ 1.04\,\frac{\mathrm{A}}{\mathrm{V}} \cdot U - 832\,\mathrm{A}, & 750\,\mathrm{V} < U \le 800\,\mathrm{V} \\ 0\,\mathrm{A}, & else \end{cases} \tag{B.3}$$

Data availability

The data used in this study were partially derived from confidential sources. While the relevant data are described in the manuscript, certain datasets cannot be shared publicly due to confidentiality agreements.

Table A.1
Overview of the implemented fuzzy control rules.

Rule	IF		THEN	
	SoC_{ESS}	U_{DC}	$i_{AIC,offset}$	$p_{EVSE,scale}$
1	Very Low	Very Low	max. Down	max. Discharge
2	Low	Very Low	max. Down	max. Discharge
3	Medium	Very Low	max. Down	max. Discharge
4	High	Very Low	max. Down	max. Discharge
5	Very High	Very Low	max. Down	max. Discharge
6	Very Low	Low	max. Down	Discharge
7	Low	Low	max. Down	Discharge
8	Medium	Low	Down	Off
9	High	Low	Down	Off
10	Very High	Low	Down	Off
11	Very Low	Medium	Down	Off
12	Low	Medium	Down	Off
13	Medium	Medium	Down	Charge
14	High	Medium	Down	Charge
15	Very High	Medium	Down	Charge
16	Very Low	High	Zero	Off
17	Low	High	Zero	Off
18	Medium	High	Zero	Charge
19	High	High	Zero	max. Charge
20	Very High	High	Zero	max. Charge
21	Very Low	Very High	Zero	Off
22	Low	Very High	Zero	Charge
23	Medium	Very High	Zero	max. Charge
24	High	Very High	Zero	max. Charge
25	Very High	Very High	Zero	max. Charge

References

[1] Borcherding H, Fosselmann E, Kuhlmann T, Stammberger H. Direct current power for sustainable factories. Tech. rep., Lyoner Strasse 9, 60528 Frankfurt am Main, Germany: ZVEI - German Electrical and Electronic Manufacturers Association; 2020.

[2] Kuhlmann T, Spanier P, Ehlich M. Potenziale einer industriellen Gleichstromversorgung [Potential of an industrial direct current supply]. In: Sauer A, editor. Die Gleichstromfabrik. München: Carl Hanser Verlag GmbH & Co. KG; 2020, p. 9–35. http://dx.doi.org/10.3139/9783446466128.

[3] Schaab DA, Weckmann S, Kuhlmann T, Sauer A. Simulative analysis of a flexible, robust and sustainable energy supply through industrial smart-DC-grid with distributed grid management. Procedia CIRP 2018;69:366–70. http://dx.doi.org/10.1016/j.procir.2017.11.037, 25th CIRP Life Cycle Engineering (LCE) Conference, 30 April – 2 May 2018, Copenhagen, Denmark.

[4] Zhao Z, Hu J, Chen H. Bus voltage control strategy for low voltage DC microgrid based on AC power grid and battery. In: 2017 IEEE international conference on energy internet. ICEI, 2017, p. 349–54. http://dx.doi.org/10.1109/ICEI.2017.68.

[5] Dragičević T, Lu X, Vasquez JC, Guerrero JM. DC microgrids—Part I: A review of control strategies and stabilization techniques. IEEE Trans Power Electron 2016;31(7):4876–91. http://dx.doi.org/10.1109/TPEL.2015.2478859.

[6] Spielmann V, Bettinger C, Skau K, Beck H-P, Fuchs C. Auswirkungen der Anreizsysteme für private PV-Anlagenbetreiber auf das lokale Verteilnetz [Impact of incentive schemes for private PV system operators on the local distribution grid]. In: Schulz D, editor. Nachhaltige Energieversorgung und Integration von Speichern. Wiesbaden: Springer Fachmedien Wiesbaden; 2015, p. 27–33. http://dx.doi.org/10.1007/978-3-658-10958-5.

[7] Eckert F, Thema M. Speicherintegration in einzelnen energiesektoren [Storage integration in individual energy sectors]. In: Sterner M, Stadler I, editors. Energiespeicher - Bedarf, Technologien, Integration. 2nd ed.. Springer Vieweg Berlin, Heidelberg; 2017, p. 685–767. http://dx.doi.org/10.1007/978-3-662-48893-5.

[8] Meschede H, Knorr L. On the impact of various mobility concepts on integrated energy systems. E-Prime - Adv Electr Eng Electron Energy 2025;13:101041. http://dx.doi.org/10.1016/j.prime.2025.101041.

[9] Stephan A, Gschwendtner C. Enabling Flexible Electric Vehicle Grid Integration. Tech. rep., CH-3003 Bern: Swiss Federal Office of Energy SFOE - Energy Research and Cleantech; 2023.

[10] Fasthuber D. Integration der Ladeinfrastruktur in das elektrische Energiesystem [Integration of charging infrastructure into the electrical energy system]. Elektrotech. Inf.tech. 2020;137(4):156–60. http://dx.doi.org/10.1007/s00502-020-00806-9.

[11] Weiß A, Müller M, Franz S. Spitzenlastkappung durch uni- und bidirektionales Laden von Elektrofahrzeugen und Analyse der resultierenden Netzbelastung in Verteilnetzen [Peak load clipping through uni- and bidirectional charging of electric vehicles and analysis of the resulting grid load in distribution grids]. Forsch Im Ingenieurwesen 2021;85(2):469–76. http://dx.doi.org/10.1007/s10010-020-00424-z.

[12] Vertgewall CM, Wehbring N, Ulbig A. Netzintegration [network integration]. In: Kampker A, Heimes HH, editors. Elektromobilität - Grundlagen einer Fortschrittstechnologie. 3rd ed.. Springer Vieweg Berlin, Heidelberg; 2023, p. 497–519. http://dx.doi.org/10.1007/978-3-662-65812-3.

[13] Gschwendtner C, Sinsel SR, Stephan A. Vehicle-to-X (V2X) implementation: An overview of predominate trial configurations and technical, social and regulatory challenges. Renew Sustain Energy Rev 2021;145:110977. http://dx.doi.org/10.1016/j.rser.2021.110977.

[14] Shafiullah M, Refat AM, Haque ME, Chowdhury DMH, Hossain MS, Alharbi AG, Alam MS, Ali A, Hossain S. Review of recent developments in microgrid energy management strategies. Sustainability 2022;14(22). http://dx.doi.org/10.3390/su142214794.

[15] Khan MW, Li G, Wang K, Numan M, Xiong L, Huang S, Khan MA. Agents-based energy scheduling of EVs and smart homes in smart grid. In: Appasani B, Bizon N, editors. Smart grid 3.0: Computational and communication technologies. Cham: Springer International Publishing; 2023, p. 185–219. http://dx.doi.org/10.1007/978-3-031-38506-3_8.

[16] Dicorato M, Forte G, Marasciuolo F, Cavarretta MC, De Michino D. Enabling optimal vehicle-to-grid operation in a DC microgrid. In: 2023 IEEE international conference on environment and electrical engineering and 2023 IEEE industrial and commercial power systems europe (EEEIC / i&cPS europe). 2023, p. 1–5. http://dx.doi.org/10.1109/EEEIC/ICPSEurope57605.2023.10194813.

[17] Dicorato M, Tricarico G, Marasciuolo F, Forte G, Trovato M. Performance analysis of EV stations optimal operation in DC microgrid configurations. In: 2020 IEEE international conference on environment and electrical engineering and 2020 IEEE industrial and commercial power systems europe (EEEIC / i&cPS europe). 2020, p. 1–6. http://dx.doi.org/10.1109/EEEIC/ICPSEurope49358.2020.9160758.

[18] Bruinsma G, Carati EG, Piveta M, Salvatti GA, Rech C. Electric vehicle charging strategy in smart grids with distributed generation. In: 2022 14th seminar on power electronics and control. SEPOC, 2022, p. 1–6. http://dx.doi.org/10.1109/SEPOC54972.2022.9976416.

[19] Shakeel FM, Malik OP. Fuzzy based energy management system for a micro-grid with a V2G parking lot. In: 2020 IEEE electric power and energy conference. EPEC, 2020, p. 1–5. http://dx.doi.org/10.1109/EPEC48502.2020.9320112.

[20] García-Triviño P, Fernández-Ramírez LM, Torreglosa JP, Jurado F. Fuzzy logic control for an electric vehicles fast charging station. In: 2016 international symposium on power electronics, electrical drives, automation and motion. SPEEDAM, 2016, p. 1099–103. http://dx.doi.org/10.1109/SPEEDAM.2016.7525924.

[21] García-Triviño P, Torreglosa JP, Fernández-Ramírez LM, Jurado F. Decentralized fuzzy logic control of microgrid for electric vehicle charging station. IEEE J Emerg Sel Top Power Electron 2018;6(2):726–37. http://dx.doi.org/10.1109/JESTPE.2018.2796029.

[22] Börchers L, Stötzer F, Becker T, Hanfeld M, Schwarz J. A simulation-based study for estimating the V2G potentials for and effects on autarky in German energy communities and quarters. Energy 2025;334:137541. http://dx.doi.org/10.1016/j.energy.2025.137541.

[23] Rehman MA, Numan M, Tahir H, Rahman U, Khan MW, Iftikhar MZ. A comprehensive overview of vehicle to everything (V2X) technology for sustainable EV adoption. J Energy Storage 2023;74:109304. http://dx.doi.org/10.1016/j.est.2023.109304.

[24] Türkoğlu AS, Güldorum HC, Sengor I, Çiçek A, Erdinç O, Hayes BP. Maximizing EV profit and grid stability through virtual power plant considering V2G. Energy Rep 2024;11:3509–20. http://dx.doi.org/10.1016/j.egyr.2024.03.013.

[25] Li P, Hu W, Xu X, Huang Q, Liu Z, Chen Z. A frequency control strategy of electric vehicles in microgrid using virtual synchronous generator control. Energy 2019;189:116389. http://dx.doi.org/10.1016/j.energy.2019.116389.

[26] Guo Y, Xing J, Zheng Q, Di S, Shi Z, Sun H. V2G auxiliary frequency regulation control strategy based on state-of-charge change and user requirements. Results Eng 2025;26:104901. http://dx.doi.org/10.1016/j.rineng.2025.104901.

[27] Blank F, Graf H, Knapp J, Schaab D, Wunder B. Netzregelung und Stabilität - Regelkennlinien [Grid control and stability – droop control characteristic]. In: Austermann J, Stammberger H, editors. Systemkonzept DC-INDUSTRIE2. 3rd ed.. Lyoner Straße 9, 60528 Frankfurt am Main: ZVEI & Konsortium DC-INDUSTRIE2; 2023, p. 77–83.

[28] Austermann J, Ehlich M, Fosselmann E, Hovestadt W, Saele J, Stammberger H, Wunder B, Unru A. Spannungswerte und Spannungsbänder [Voltage values and voltage ranges]. In: Austermann J, Stammberger H, editors. Systemkonzept DC-INDUSTRIE2. 3rd ed.. Lyoner Straße 9, 60528 Frankfurt am Main: ZVEI & Konsortium DC-INDUSTRIE2; 2023, p. 40–8.

[29] Ehlich M, Austermann J, Blank F, Borcherding H, Weis B. Systemkonzept eines fabrikinternen DC-Netzes [System concept for an in-house DC grid]. In: Sauer A, editor. Die Gleichstromfabrik. München: Carl Hanser Verlag GmbH & Co. KG; 2020, p. 71–114. http://dx.doi.org/10.3139/9783446466128.

[30] Ott L, Schaab D, Männel A, Hinderer W. Netzmanagement [network management]. In: Sauer A, editor. Die Gleichstromfabrik. München: Carl Hanser Verlag GmbH & Co. KG; 2020, p. 115–38. http://dx.doi.org/10.3139/9783446466128.

[31] Klein K, Kalz D, Herkel S. Netzdienlicher Betrieb von Gebäuden: Analyse und Vergleich netzbasierter Referenzgrößen und Definition einer Bewertungskennzahl [Grid-serving operation of buildings: Analysis and comparison of grid-based reference values and definition of an evaluation indicator]. Bauphysik 2014;36(2):49–58. http://dx.doi.org/10.1002/bapi.201410019.

[32] Riegel B, Ohms D, Cattaneo E, Langer G, Herrmann M. Elektrochemische energiespeicher [Electrochemical energy storage systems]. In: Sterner M, Stadler I, editors. Energiespeicher - Bedarf, Technologien, Integration. 2nd ed.. Springer Vieweg Berlin, Heidelberg; 2017, p. 229–326. http://dx.doi.org/10.1007/978-3-662-48893-5.

[33] Krauter S, Zhang L. Correlation of grid-frequency, electricity prices, share of renewable, and CO2—contents in the German electricity grid to enable inexpensive triggering of demand—Side—Management. In: 2020 47th IEEE photovoltaic specialists conference. PVSC, 2020, p. 1672–4. http://dx.doi.org/10.1109/PVSC45281.2020.9300487.

[34] Klein K, Langner R, Kalz D, Herkel S, Henning H-M. Grid support coefficients for electricity-based heating and cooling and field data analysis of present-day installations in Germany. Appl Energy 2016;162:853–67. http://dx.doi.org/10.1016/j.apenergy.2015.10.107.

[35] Lee ZJ, Li T, Low SH. ACN-Data: Analysis and applications of an open EV, charging dataset. In: Proceedings of the tenth international conference on future energy systems. E-energy '19, 2019.

[36] Kraftfahrt-Bundesamt [Federal Motor Transport Authority]. Neuzulassungen von Personenkraftwagen nach Marken und Modellreihen im Oktober 2023 [New passenger car registrations by brand and model series in October 2023]. 24932 Flensburg: Kraftfahrt-Bundesamt; 2023, URL https://www.kba.de/DE/Statistik/Produktkatalog/produkte/Fahrzeuge/fz10/fz10_gentab.html.

[37] Database EV. Nutzbare Batteriekapazität von Elektroautos [Usable battery capa of electric cars]. TNW West - Tower 4, Kon. Wilhelminaplein 1, 1062 HG Amsterdam; 2023 URL https://ev-database.org/de/cheatsheet/useable-battery-capa-electric-car.

[38] Krug S, Krey O, Ohm B, Braune O, Weider M. Elektromobilität vor Ort [Local electric mobility]. Tech. rep., Fasanenstraße 5, 10623 Berlin: NOW GmbH Nationale Organisation Wasserstoff- und Brennstoffzellentechnologie; 2018.

[39] Sagaria S, van der Kam M, Boström T. Vehicle-to-grid impact on battery degradation and estimation of V2G economic compensation. Appl Energy 2025;377:124546. http://dx.doi.org/10.1016/j.apenergy.2024.124546.

[40] The Mobility House GmbH. Optimizing battery lifespan: How vehicle-to-grid and smart charging influence EV battery aging. Tech. rep., St.-Cajetan-Str. 43, 81669 Munich: The Mobility House GmbH; 2025.

[41] Nickel S, Rebennack S, Stein O, Waldmann K-H. Operations Research. 3rd ed.. Springer Gabler Berlin, Heidelberg; 2022, http://dx.doi.org/10.1007/978-3-662-65346-3.

[42] BDEW eV. Hinweise zu den akualisierten Standardlastprofilen Strom [Notes on the updated standard load profiles for electricity]. Tech. rep., Reinhardtstraße 32, 10117 Berlin, Germany: BDEW Bundesverband der Energie- und Wasserwirtschaft e.V.; 2025.

[43] Zemin D, Yueming L, Zhicheng Y, Youhong Y, Yongbao L. Coordinated control strategy of engine-grid-load-storage for shipboard micro gas turbine DC power generation system: A review. J Energy Storage 2025;134:118205. http://dx.doi.org/10.1016/j.est.2025.118205.